Monthly Notices
of the
ROYAL ASTRONOMICAL SOCIETY

MNRAS **490,** 1944–1952 (2019)
Advance Access publication 2019 October 12

doi:10.1093/mnras/stz2757

New observational constraints on interacting dark energy using galaxy clusters virial equilibrium states

M. Le Delliou,[1,2,3]★ R. J. F. Marcondes[4] and G. B. Lima Neto[5]

[1]*Institute of Theoretical Physics, School of Physical Science and Technology, Lanzhou University, No. 222, South Tianshui Road, Lanzhou, Gansu 730000, P. R. China*
[2]*Instituto de Astrofísica e Ciências do Espaço, Universidade de Lisboa, Faculdade de Ciências, Ed. C8, Campo Grande, P-1769-016 Lisboa, Portugal*
[3]*Instituto de Física Teórica, Universidade Estadual de São Paulo (IFT-UNESP), Rua Dr. Bento Teobaldo Ferraz 271, Bloco 2 – Barra Funda, CEP 01140-070 São Paulo, SP, Brazil*
[4]*Instituto de Física, Universidade de São Paulo, Rua do Matão 1371, Cidade Universitária, CEP 05508-090 São Paulo, SP, Brazil*
[5]*Instituto de Astronomia, Geofísica e Ciências Atmosféricas, Universidade de São Paulo, Rua do Matão 1226, Cidade Universitária, CEP 05508-090 São Paulo, SP, Brazil*

Accepted 2019 September 26. Received 2019 August 30; in original form 2018 November 26

ABSTRACT

The nature of the dark sector components of the Universe still remains one of the largest unknown. Among many possibilities, it has been speculated that dark matter and dark energy may be more tightly coupled than usually thought, one component interacting with the other. Here, we continue to explore the possible dark sector interaction through means of the Layzer–Irvine equation together with a model of an interacting dark sector applied to clusters of galaxies. We have selected galaxy clusters that have their mass profiles determined by gravitational lensing effect (optical observations) and have their intracluster gas temperatures measured from X-ray observations and spectral fit found in the literature. Using a simple model based on semi-analytical simulations, we derived a putative dynamical evolution of the clusters and used it to estimate the coupling parameter of the dark sector interaction. Through a Bayesian analysis, we obtain a 3σ detection of the interaction strength for 11 clusters at -0.027 ± 0.009 that translates in a compounded Universal equilibrium virial ratio, U/T, of $-0.61^{+0.04}_{-0.03}$. We note that the X-ray temperature determination is sometimes inconsistent, depending on the instrument and/or methodology used. The level of detection and these inconsistencies call for caution. We expect that future observations will give us a clearer indication of an eventual dark sector interaction.

Key words: gravitation – galaxies: clusters: general – cosmology: theory – dark energy – dark matter – large-scale structure of Universe.

1 INTRODUCTION

Since the discovery of cosmic acceleration (Perlmutter et al. 1999) and the proposal of dark energy (DE) as its source, in addition to the already sought dark matter (DM; Zwicky 1933, 1937), the largely unknown nature of the dark sector naturally called for possible interactions within its manifestations (Amendola 2000a,b).

Despite considerable efforts towards direct and indirect detection, the only evidence at hand of the existence of the dark sector remain purely gravitational, through the Cosmic Microwave Background observations (Ade et al. 2014), supernovae acceleration (Perlmutter et al. 1999; Riess et al. 1998) or clusters displaying segregated mass and baryons (dissociative clusters), such as the so-called Bullet Cluster (Clowe et al. 2006), El Gordo (Jee et al. 2014), Abell 1758 (Monteiro-Oliveira et al. 2017), among others. In this context, detection of interactions within the dark sector would significantly help us understand the nature of DM and DE and, of course, add evidence for the very existence of these two elusive components.

In a previous paper (Le Delliou et al. 2015, hereafter LeD15), we developed an approach to the detection of such interactions in the virial state of galaxy clusters, through a simplified coupled dark energy (CDE) cosmology model, coupled with the Layzer–Irvine dynamical virial equation. Based on a series of papers exploring such detection in apparently balanced clusters, and their check by other groups (Bertolami, Gil Pedro & Le Delliou 2007; Le Delliou, Bertolami & Gil Pedro 2007; Bertolami, Gil Pedro & Le Delliou 2008, 2009, 2012; Abdalla et al. 2009; Abdalla, Abramo & de Souza 2010; He et al. 2010), this latest approach attempted to include the effect of departure from equilibrium (DfE). However, although this allowed for the use in the detection of a wider sample of clusters, it involved the assumption that clusters present small departures from

★ E-mail: morgan.ledelliou.ift@gmail.com

virial equilibrium and found it to be the source of inconsistencies in the results. This paper proposes now to remedy these inconsistencies by allowing larger departures in an evaluation independent from the astrophysical processes expected to source this deviation from balance. We also attempt a more robust statistical treatment of the data, with a Bayesian approach.

This paper is organized as follows. In Section 2, we describe the framework in which data are analysed. The sample and statistical treatment are discussed in Section 3.1, while the analysis is described in Section 4. The results are discussed in Section 5 before to conclude in Section 6.

2 THE FRAMEWORK

2.1 The cosmological model

We model the universe, composed of DM and DE only, as a flat Friedmann–Lemaître–Robertson–Walker (FLRW) background metric. The dark sector interaction is modelled with a heat flux in the Bianchi identities between the two dark components, denoted by subscript c for cold DM and d for DE (i.e. energy conservation equations, linking the energy densities ρ evolutions, the DE equation of state $w_\mathrm{d} = P_\mathrm{d}/\rho_\mathrm{d}$, P_d being the DE pressure, and the Hubble parameter H to the DM–DE interaction coupling ξ):

$$\dot{\rho}_\mathrm{c} + 3H\rho_\mathrm{c} = 3H\xi\rho_\mathrm{c}, \qquad \dot{\rho}_\mathrm{d} + 3H\rho_\mathrm{d}(1+w_\mathrm{d}) = -3H\xi\rho_\mathrm{c}. \quad (1)$$

With this sign convention, positive ξ means that DE decays into DM. The equation-of-state parameter w_d is set to -1 in most of our analyses, except in one case where we make it a free parameter of the model. The rest of the FLRW evolution is standard. This interacting model, of which idea is based on Amendola (2000a), has been largely used in this simplified form by, e.g. Bertolami et al. (2007), Bertolami et al. (2009), Feng et al. (2008), Caldera-Cabral, Maartens & Schaefer (2009), Abdalla et al. (2009), Abdalla et al. (2010), Majerotto, Väliviita & Maartens (2010), He et al. (2010), He, Wang & Abdalla (2011), Bertolami et al. (2012), Cao & Liang (2013), Salvatelli et al. (2013), Le Delliou et al. (2015), Costa et al. (2017), and is considered sufficient to capture the essential effect of the Amendola (2000a) model[1] for the purpose of studying its effect on virial balance, including the simplifying assumption of taking $w_\mathrm{d} = -1$ (Amendola et al. 2013; Wang et al. 2016). This value of w_d corresponds as well to that of the concordance model from observations (e.g. Ade et al. 2014), i.e. the cosmological constant, and allows for easier comparison in the future of our results with the literature.

2.2 The Layzer–Irvine equation

The Layzer–Irvine equation can be recasted to relate the kinetic (ρ_K) and gravitational potential (ρ_W) parts of the DM density ρ_c of the studied, evolving system (a cluster). As a generalization of the virial equation, it describes how the system tends to relax. Within this CDE scenario, it has been obtained by Bertolami et al. (2007) and He et al. (2010) as

$$\dot{\rho}_\mathrm{c} + H\left[(2+3\xi)\,\rho_\mathrm{K} + (1-6\xi)\,\rho_\mathrm{W}\right] = 0. \quad (2)$$

Note that the densities in the Layzer–Irvine equation are average densities of inhomogeneous distributions and that the interaction term density dependence here becomes inhomogeneous and integrated in the same way. In LeD15,[2] the condition of small departures from equilibrium was imposed that led to the approximation $\dot{\rho}_\mathrm{K}/\rho_\mathrm{K} \simeq \dot{\rho}_\mathrm{W}/\rho_\mathrm{W}$. In this work, the results from LeD15 require to allow the clusters to be away from equilibrium. Thus, $\dot{\rho}_\mathrm{W}$ and $\dot{\rho}_\mathrm{K}$ will be modelled separately (see Section 2.2.2).

Equation (2) can now be reformulated to give the out-of-equilibrium virial ratio

$$\frac{\rho_\mathrm{K}}{\rho_\mathrm{W}} = -\frac{1-6\xi}{2+3\xi} - \frac{1}{2+3\xi}\frac{\dot{\rho}_\mathrm{K}+\dot{\rho}_\mathrm{W}}{H\rho_\mathrm{W}}. \quad (3)$$

This allows us to compare observed values of the virial ratio, built from the quantity $\rho_\mathrm{K}/\rho_\mathrm{W}$ extracted from clusters and called hereafter the observed virial ratio (OVR), with a modified ratio involving the interaction coupling, which we will refer to as the equilibrium virial ratio (EVR),[3] and the time evolution term involving the time derivative, which we call DfE. We propose to model and build the OVR and DfE from observations of clusters' mass M_{200} enclosed in a radius r_{200},[4] a concentration parameter c_{200} and the X-ray temperature T_X. The DfE will also depend on the parameter of interest ξ, on the density parameter Ω_{c0}, and on $h \equiv H_0/100\,\mathrm{km\,s^{-1}\,Mpc^{-1}}$ that enter in the Hubble rate H. Rewriting equation (3) as

$$\frac{\rho_\mathrm{K}}{\rho_\mathrm{W}} + \frac{1}{2+3\xi}\frac{\dot{\rho}_\mathrm{K}+\dot{\rho}_\mathrm{W}}{H\rho_\mathrm{W}} = -\frac{1-6\xi}{2+3\xi}, \quad (4)$$

explicit the Universal, predicted EVR (i.e. the kinetic to potential ratio that should be reached by a cluster at perfect equilibrium) that can be obtained from specific clusters' OVR minus DfE in the left-hand side of equation (4). The first step is to evaluate the kinetic and potential energy densities. Then we need to evaluate in a sensible way the DfE term. Thus, only remains to place constraints on the interaction coupling parameter ξ, which can be performed by Markov Chain Monte Carlo (MCMC) simulations.

2.2.1 *The kinetic and potential energy densities*

We follow LeD15 evaluations of these densities from the measurements of the given cluster's X-ray temperature T_X, mass M_{200}, and Navarro–Frenk–White (NFW) concentration parameter c_{200}. The potential energy is approximated using the NFW density profile (Navarro, Frenk & White 1996) extracted from the cluster's observed mass and concentration (defining $c_{200} = r_{200}/r_0$ instead of using r_0). Thus, we have

$$\rho_\mathrm{W} = -\frac{3GM_{200}^2}{4\pi r_{200}^4 f_\mathrm{c}}, \quad (5)$$

[1] Note that other coupling, similar to Amendola (2000a) or not, can also be proposed (e.g. Böhmer et al. 2008; Li & Zhang 2011).

[2] In LeD15, the choice of the coupling strengths $\xi_1 = \xi/18$ and $\xi_2 = -(\xi/6)\,\rho_\mathrm{c}/\rho_\mathrm{d}$ was inconsistent with the derivation of the Layzer–Irvine equation by He et al. (2010), which defines ξ_1 and ξ_2 to be constants. Here, we amend that inaccuracy by simply adopting $\xi_1 = \xi$ and $\xi_2 = 0$, which also makes the interaction dependent on the DM energy density only, but leads to a different Layzer–Irvine equation. Notice that the sign of the interacting term yields a positive flux $3H\xi\rho_\mathrm{c}$ towards DM when all terms are positive, making the arbitrary choice followed by some phenomenological descriptions of the interacting term in the literature (for instance, He et al. 2010; Cao & Liang 2013; Costa et al. 2017).

[3] Formerly named theoretical virial ratio (TVR) in LeD15.

[4] Recall then that $M_{200}/\mathrm{Vol}(r_{200}) = 200\,\rho_\mathrm{cr}$ with the critical density $\rho_\mathrm{cr} = 3H^2(z)/8\pi G$.

with

$$f_c \equiv \frac{C^2/c_{200}}{\frac{1}{2}c_{200}^2 - C}, \quad C \equiv C' \ln C' - c_{200}, \quad C' \equiv 1 + c_{200}\,. \tag{6}$$

The kinetic energy is (LeD15)

$$\rho_{\rm K} = \frac{9}{8\pi}\frac{M_{200}}{r_{200}^3}\frac{k_{\rm B}T_{\rm X}}{\mu m_{\rm H}}\,, \tag{7}$$

where $k_{\rm B}$ is the Boltzmann constant, $\mu = 0.63$ is the intracluster plasma mean molecular weight (defined as the mean mass of the particles divided by the Hydrogen mass, assumed to be completely ionized and with primordial chemical composition), and $m_{\rm H}$ is the proton mass.

Here, we maintain the LeD15 proxy of cluster kinetic energy by $T_{\rm X}$, as analyses such as Mainini (2005), Mainini & Bonometto (2006), Le Delliou & Barreiro (2013), and Liao et al. (2017) lead us to expect a small segregation of baryons for non-extremal models. Moreover, hydrodynamical simulations (as seen in Rasia, Tormen & Moscardini 2004; Baldi et al. 2010) and some considerations on reaching energy equipartition, e.g. through dynamical friction (Del Popolo 2009), provide reasonable grounds to consider baryons kinetic state to be good tracer of total mass kinetic energy. The ratio of these two densities is the OVR

$$\frac{\rho_{\rm K}}{\rho_{\rm W}} = -\frac{3}{2}\frac{r_{200}}{GM_{200}}\frac{k_{\rm B}T_{\rm X}}{\mu m_{\rm H}} f_{\rm c}. \tag{8}$$

The radius r_{200} is evaluated from the NFW parameters (see footnote 4) with the critical density at the redshift of the cluster and in the same cosmology assumed by the observers to keep consistency with the fitted NFW profile.

2.2.2 *Evaluating the DfE*

To allow for the extra freedom introduced by relaxing the small departures from equilibrium assumption, compared to LeD15, the virial ratio now depends on both temperature and virial radius, the concentration remaining a parameter derived from the observed NFW density profile (Section 3.1). We note that both densities can be rewritten as functions of their local measured quantities, recognizing the critical density ratio definition in powers of mass and radius, as

$$\rho_{\rm K} = \rho_{\rm K}(T_{\rm X}) = 300\,\rho_{\rm cr}\frac{k_{\rm B}T_{\rm X}}{\mu m_{\rm H}} \tag{9}$$

and

$$\rho_{\rm W} = \rho_{\rm W}(r_{200}) = -\,(200\,\rho_{\rm cr})^2\,G\frac{4\pi}{3}\frac{r_{200}^2}{f_{\rm c}}. \tag{10}$$

We thus can compute the time derivatives of equation (3) as

$$\dot\rho_{\rm K} + \dot\rho_{\rm W} = \frac{{\rm d}\rho_{\rm K}}{{\rm d}T_{\rm X}}\dot T_{\rm X} + \frac{{\rm d}\rho_{\rm W}}{{\rm d}r_{200}}\dot r_{200}, \tag{11}$$

which is fully general, as opposed to the evaluation in LeD15. The delicate part is then to evaluate $\dot T_{\rm X}$ and $\dot r_{200}$. Based on the reasonable expectations from hierarchical structure formation that clusters' temperature and radius should evolve to equilibrium values, increasing faster in the past than in the future, we propose two physically reasonable ansätze that derivatives asymptote to zero from positive decreasing values, meaning that both $T_{\rm X}$ and r_{200} should increase to reach equilibrium. Such behaviour can be observed in semi-analytical simulations (as can be seen from the studies of Henriksen & Widrow 1995, 1997, 1999; Del Popolo et al. 2000; Le Delliou & Henriksen 2003; MacMillan, Widrow & Henriksen 2006; Le Delliou 2008). Although cosmological N-body and smooth particle hydrodynamic (SPH) simulations are usually unable to provide the isolated behaviour of haloes (Macciò et al. 2004; Baldi et al. 2010; Baldi 2012), the semi-analytical infall model explains generic features and behaviours of haloes. In particular, the model developed by Henriksen & Widrow (1995), Henriksen & Widrow (1997), Henriksen & Widrow (1999), and extended in various works such as Del Popolo et al. (2000), Le Delliou & Henriksen (2003), MacMillan et al. (2006), Le Delliou (2008) has been shown to contain all the physical behaviours observed in fully numerical simulations, including such characteristics as their NFW (Navarro et al. 1996) density profiles (Del Popolo et al. 2000; Le Delliou & Henriksen 2003), or their typical repeated merger mass acquisition (Le Delliou 2008). In particular, fig. 5 of Henriksen & Widrow (1999) clearly shows the sharp increase until quasi-equilibrium of self-similar mass and radius of the system, and together with figs 3–5 of Le Delliou & Henriksen (2003) or figs 1–3 of Le Delliou (2008), how the smooth accretion of mass pushes towards a quasi-virial equilibrium that very quickly relaxes to the usual virial when the system becomes isolated. Figs 1–3 of Le Delliou (2008) demonstrate the effect of non-smooth mergers on the quasi-equilibrium state. Put together, these behaviours vindicate our choice of the following ansätze:

$$\dot T_{\rm X} = \frac{T_{\rm X}/t_0}{(t/t_0)^2}, \quad \dot r_{200} = \gamma\frac{r_{200}/t_0}{(t/t_0)^{\gamma+1}}, \tag{12}$$

derived, respectively, from heuristic exponential parametrizations $T_{\rm X} = T_{\rm X}^*\exp(-t_0/t)$ and $r_{200} = r_{200}^*\exp(-(t_0/t)^\gamma)$ ($\gamma \neq 1$), where $T_{\rm X}^*$ and r_{200}^* are the asymptotic equilibrium values and t_0 is some characteristic time-scale. The parametrization is using the simplicity of the strong convergence of the exponential function (see e.g. the fast virialization of haloes seen in Henriksen & Widrow 1999, and their moderately violent relaxation) and the finite value convergence of the inverse power law. We further restrict our parametrization of γ to positive values so as to keep the approach of asymptotic growth of the radius towards r_{200}^*. When $\gamma < 1$ ($\gamma > 1$), the radius approaches the equilibrium faster (slower) than the temperature.[5] These ansätze are used locally to give the evolution slopes but are not considered globally integrable. They provide one equation,

$$\frac{\dot T_{\rm X}}{T_{\rm X}/t_0} = \left(\frac{\dot r_{200}}{\gamma r_{200}/t_0}\right)^{\frac{2}{\gamma+1}}, \tag{13}$$

to obtain the unknown time evolutions $\dot T_{\rm X}$ and $\dot r_{200}$. The remaining equation needed to provide a solution in terms of observed values for these unknown can be chosen as the equation of state for the perfect gas, considered isobaric:

$$\frac{T_{\rm X}}{r_{200}^3} = \text{constant}, \tag{14}$$

which can be derived into

$$\frac{\dot T_{\rm X}}{\dot r_{200}} = 3\frac{T_{\rm X}}{r_{200}}. \tag{15}$$

Solving for the derivatives in terms of γ, $T_{\rm X}$, and r_{200}, the DfE term is given by

$$-\frac{\dot\rho_{\rm K} + \dot\rho_{\rm W}}{(2+3\xi)\,H\rho_{\rm W}} = -\left(3\frac{T_{\rm X}}{\rho_{\rm W}}\frac{{\rm d}\rho_{\rm K}}{{\rm d}T_{\rm X}} + \frac{r_{200}}{\rho_{\rm W}}\frac{{\rm d}\rho_{\rm W}}{{\rm d}r_{200}}\right)\frac{\left(\gamma^2 3^{\gamma+1}\right)^{\frac{1}{1-\gamma}}}{(2+3\xi)\,Ht_0}, \tag{16}$$

[5]The two cases are better analysed separately due to divergences at $\gamma = 1$. For the sake of simplicity, in this work we consider only the first case.

with the derivatives given by

$$\frac{T_X}{\rho_W}\frac{d\rho_K}{dT_X} = \frac{\rho_K}{\rho_W}\frac{d\ln\rho_K}{d\ln T_X} = \frac{\rho_K}{\rho_W} \tag{17}$$

and

$$\frac{r_{200}}{\rho_W}\frac{d\rho_W}{dr_{200}} = 2 - \frac{d\ln f_c}{d\ln r_{200}} = 2 - \frac{d\ln f_c}{d\ln c_{200}}. \tag{18}$$

The exact time-scale t_0 is not important to our purposes. Since this parameter only appears dividing $(\gamma^2 3^{\gamma+1})^{1/(1-\gamma)}$, it can be absorbed into this term with the only effect of shifting the value of γ at which its marginalized distribution becomes suppressed (as that term diverges with γ approaching the unity), so we set $t_0 = 1$ (in units of $\mathrm{km^{-1}\,s\,Mpc}$).

3 THE DATA

We start from a sample of 50 clusters with weak-lensing mass measurements of M_{200} given by Okabe & Smith (2016) and corresponding measurements of c_{200} kindly provided by Okabe [private communication, as they were obtained at the same time as Okabe & Smith (2016) but remained unpublished]. Note that both parameters, M_{200} and c_{200}, are obtained by a fitting procedure, so do not derive from any c_{200}–M_{200} scaling relation. Therefore, the eventual dependence of the c_{200}–M_{200} on the coupling between DE and DM (as showed by the N-body simulations of Baldi et al. 2010; Li & Barrow 2011a, b) will not alter our results.

The NFW profiles are based on a flat ΛCDM background cosmology with DM and DE density parameters $\Omega_{c0} = 0.3$ and $\Omega_{d0} = 0.7$, which we use in the evaluation of r_{200}. These data can be complemented with X-ray temperature data from a few different sources. By collecting temperature data from Maughan et al. (2012), Martino et al. (2014) or Mantz et al. (2016), Mantz et al. (2017) (hereafter M12, M14, and M16, respectively), we end up with subsets of 22, 19, or 30 clusters. The data are summarized in Table 1.

We note that uncertainties in M_{200}, c_{200}, and $k_B T_X$ from M12 are generally asymmetrical, in the form $\bar{x}^{+\sigma_+}_{-\sigma_-}$. Since these quantities should be always positive and typically $\sigma_+ \geq \sigma_-$, it seems reasonable to assume that these 1σ-error measurements represent well 68.3 per cent credible intervals of lognormal distributions. As in LeD15, we want these lognormal distributions to have their parameters μ and σ adjusted to match the following conditions: (i) the maximum probability coincides with the nominal value $\bar{x}$, (ii) the probability of the random variable lying between $\bar{x} - \sigma_-$ and $\bar{x} + \sigma_+$ is 68.3 per cent and (iii) the probability density function has the same value at the points $\bar{x} - \sigma_-$ and $\bar{x} + \sigma_+$, so that the interval between them corresponds to the 68.3 per cent most likely values. For this, we write

$$\chi^2 = C^2_{(i)} + C^2_{(ii)} + C^2_{(iii)}, \tag{19}$$

where

$$C_{(i)} \equiv \frac{\exp(\mu - \sigma^2)}{\bar{x}} - 1, \tag{20}$$

$$C_{(ii)} \equiv \frac{f_{\mu,\sigma}(\bar{x} + \sigma_+)}{f_{\mu,\sigma}(\bar{x} - \sigma_-)} - 1, \tag{21}$$

$$C_{(iii)} \equiv \frac{F_{\mu,\sigma}(\bar{x} + \sigma_+) - F_{\mu,\sigma}(\bar{x} - \sigma_-)}{0.683} - 1 \tag{22}$$

represent the three conditions, with

$$f_{\mu,\sigma}(x) = \frac{1}{x\sigma\sqrt{2\pi}}\exp\left[-\frac{(\ln x - \mu)^2}{2\sigma^2}\right] \tag{23}$$

and

$$F_{\mu,\sigma}(x) = \frac{1}{2}\left[1 + \mathrm{erf}\left(\frac{\ln x - \mu}{\sigma\sqrt{2}}\right)\right] \tag{24}$$

the lognormal probability (PDF) and cumulative (CDF) density functions, respectively. We then find, for each of these measurements, the pair of parameters (μ, σ) that minimizes χ^2. The parametrizations obtained are verified to match the three conditions remarkably well in all cases. We list all the fitted parameters (μ, σ) in Table 2. Since the logarithm of these distributions follow Gaussian distributions with the usual parameters (μ, σ), we proceed to use linear error propagation for the left-hand side of equation (4) with the asymmetrical measurements $\bar{x}^{+\sigma_+}_{-\sigma_-}$ symmetrized to $\bar{x}' \pm \Delta x' = \exp(\mu \pm \sigma)$ for the quantities M_{200}, c_{200}, and $k_B T_X$. Whenever possible, the error is propagated on the combined logarithmic quantities first, to minimize introduction of bias. We compute the OVRs following equation (8) and present them in Fig. 1.

The differences in OVRs reflect the different temperature measurements listed in Table 1 and also plotted in Fig. 2. In view of conflicting data, we build 'gold' samples of clusters that have at least two temperature measurements within 1σ of each other, and consider their average (or the average of their logarithms) for the calculations. By inspecting Fig. 2, we selected three gold samples composed of six clusters from M12+M14: ABELL0115, ABELL0209, ABELL0781, ABELL1763, ABELL1914, ABELL2631; one cluster from M12+M16: ABELL0586; and four clusters form M14+M16: ABELL0773, ABELL1689, ABELL1835 and ABELL2537 from overlapping error bar clusters. A sample with all eleven clusters from these samples (referred to as GOLD) is also considered.

The Hubble function $H(z)$ in the DfE term must be evaluated in the CDE cosmology, thus depending on the parameters ξ, h, and $\Omega_{c0}h^2$. In terms of these parameters, $H(z)$ is given by the Friedmann equation (restricting to the case $w_d = -1$) in the form

$$\left[\frac{H(z)}{100}\right]^2 = h^2 + \Omega_{c0}h^2\frac{a^{-3(1-\xi)} - 1}{1 - \xi}. \tag{25}$$

When w_d is free, $H(z)$ is obtained from the Friedmann equation in its original form with the numerical solutions of equations (1). We then include $H(z)$ from cosmic chronometer data (Moresco et al. 2016), the JLA supernovae binned data set (Betoule et al. 2014) and the local measurement of $H_0 = (73.24 \pm 1.74)\,\mathrm{km\,s^{-1}Mpc^{-1}}$ from Riess et al. (2016), joined to the clusters data, in order to perform the analysis outputting h and $\Omega_{c0}h^2$ together with ξ.

3.1 The clusters likelihood

The left-hand side of equation (4), computed from the measurements of mass, temperature and NFW concentration, constitutes our observable, as explained in Section 2.2. Denoting by $f_N(x;\mu,\sigma) = (2\pi\sigma^2)^{-1/2}\exp[-(x-\mu)^2/2\sigma^2]$ the PDF of a Gaussian distribution $N(\mu, \sigma)$, we assume Gaussian likelihoods $\mathcal{L}_{\rm cluster} = f_N(\mathrm{EVR};\mu,\sigma)$ for each cluster, with μ and σ given by the nominal value and standard deviation of the quantity OVR–DfE, to compare the predicted values of the EVR $\mathrm{EVR}(\xi) \equiv -(1-6\xi)/(2+3\xi)$ with this observable.

The total likelihood of a set of clusters is given by the product $\mathcal{L}_{\rm clusters} = \prod_i \mathcal{L}_{\rm cluster\,i}$ of the likelihoods of all the clusters in the given sample. We should stress that the left-hand side of equation (4) depends on the amount of matter and the Hubble parameter through Ω_{c0} and H_0, or equivalently $\Omega_{c0}h^2$ and h, motivating us to include $H(z)$ and supernovae data. The parameters ξ and γ

Table 1. Redshift, NFW parameters from Okabe & Smith (2016) and temperature of galaxy clusters from different sources. Temperatures are given in keV and masses in units of $h^{-1}10^{14}M_{\odot}$.

Cluster	z	M_{200}	c_{200}	k_BT_X (Maughan et al. 2012)	k_BT_X (Martino et al. 2014)	k_BT_X (Mantz et al. 2016, 2017)
ABELL0068	0.2546	$6.65^{+1.35}_{-1.16}$	$4.83^{+1.83}_{-1.31}$	7.8 ± 1.0	5.02 ± 1.65	9.62 ± 1.65
ABELL0115	0.1971	$7.04^{+2.66}_{-1.97}$	$1.59^{+1.12}_{-0.77}$	6.7 ± 0.3	6.46 ± 0.51	11.74 ± 0.90
ABELL0209	0.2060	$12.75^{+2.27}_{-1.91}$	$3.63^{+1.02}_{-0.84}$	7.4 ± 0.5	7.56 ± 1.40	8.98 ± 0.67
ABELL0267	0.2300	$5.96^{+1.16}_{-1.08}$	$3.16^{+1.01}_{-0.81}$	$4.4^{+0.5}_{-0.4}$	–	–
ABELL0383	0.1883	$5.23^{+1.30}_{-1.07}$	$4.12^{+2.06}_{-1.41}$	4.5 ± 0.3	5.76 ± 1.26	7.26 ± 0.42
ABELL0521	0.2475	$5.61^{+1.18}_{-1.05}$	$3.48^{+1.57}_{-1.09}$	4.8 ± 0.2	–	7.29 ± 0.25
ABELL0586	0.1710	$6.65^{+2.15}_{-1.61}$	$6.77^{+6.83}_{-3.36}$	7.6 ± 0.8	–	7.40 ± 0.53
ABELL0697	0.2820	$9.74^{+2.90}_{-2.13}$	$1.75^{+1.00}_{-0.75}$	$10.2^{+0.8}_{-0.7}$	–	14.58 ± 1.44
ABELL0750	0.1630	$6.30^{+2.71}_{-1.74}$	$3.79^{+2.72}_{-1.68}$	–	–	6.04 ± 0.38
ABELL0773	0.2170	$9.56^{+1.28}_{-1.14}$	$5.67^{+1.58}_{-1.27}$	7.4 ± 0.4	8.64 ± 2.05	8.97 ± 0.52
ABELL0781	0.2984	$6.57^{+1.97}_{-1.65}$	$2.32^{+2.16}_{-1.32}$	$5.5^{+0.7}_{-0.5}$	5.64 ± 2.22	–
ABELL0907	0.1669	$14.28^{+4.59}_{-2.99}$	$1.86^{+0.94}_{-0.72}$	5.4 ± 0.2	6.23 ± 0.45	7.17 ± 0.26
ABELL0963	0.2050	$7.13^{+1.38}_{-1.20}$	$3.77^{+1.38}_{-1.05}$	–	–	7.60 ± 0.37
ABELL1423	0.2130	$4.30^{+1.19}_{-0.97}$	$5.03^{+4.17}_{-2.30}$	–	–	7.04 ± 0.45
ABELL1682	0.2260	$8.66^{+1.38}_{-1.21}$	$3.93^{+1.00}_{-0.83}$	$5.8^{+2.0}_{-1.2}$	–	7.67 ± 0.74
ABELL1689	0.1832	$10.98^{+1.66}_{-1.46}$	$10.56^{+4.31}_{-2.81}$	$8.4^{+0.4}_{-0.3}$	11.23 ± 1.06	10.92 ± 0.32
ABELL1763	0.2279	$16.92^{+3.42}_{-2.70}$	$3.11^{+1.09}_{-0.86}$	8.1 ± 0.5	7.98 ± 1.45	9.09 ± 0.67
ABELL1835	0.2528	$10.09^{+1.88}_{-1.63}$	$6.94^{+4.29}_{-2.35}$	–	11.06 ± 1.09	12.15 ± 0.45
ABELL1914	0.1712	$8.73^{+1.92}_{-1.59}$	$2.64^{+1.03}_{-0.81}$	$8.5^{+0.6}_{-0.4}$	8.57 ± 1.57	9.67 ± 0.50
ABELL2009	0.1530	$7.78^{+3.19}_{-2.03}$	$1.96^{+1.61}_{-0.96}$	–	–	7.37 ± 0.47
ABELL2111	0.2290	$4.93^{+2.68}_{-1.48}$	$4.98^{+9.01}_{-3.92}$	$6.4^{+0.7}_{-0.6}$	–	9.07 ± 0.70
ABELL2204	0.1524	$9.56^{+2.29}_{-1.83}$	$5.17^{+2.10}_{-1.48}$	$8.4^{+0.8}_{-0.6}$	10.50 ± 1.11	14.98 ± 0.72
ABELL2219	0.2281	$10.40^{+2.15}_{-1.75}$	$2.04^{+0.99}_{-0.75}$	–	–	12.80 ± 0.36
ABELL2261	0.2240	$11.93^{+2.18}_{-1.80}$	$2.69^{+0.93}_{-0.74}$	7.3 ± 0.4	–	8.75 ± 0.49
ABELL2390	0.2329	$10.60^{+1.91}_{-1.67}$	$4.11^{+1.15}_{-0.96}$	–	–	15.47 ± 0.68
ABELL2485	0.2472	$5.72^{+1.33}_{-1.13}$	$3.44^{+2.11}_{-1.34}$	–	–	7.37 ± 0.94
ABELL2537	0.2966	$7.65^{+2.31}_{-1.90}$	$8.76^{+10.55}_{-4.29}$	–	8.68 ± 3.78	9.22 ± 0.61
ABELL2552	0.2998	$7.61^{+2.88}_{-2.08}$	$3.20^{+3.16}_{-1.76}$	–	–	10.43 ± 1.34
ABELL2631	0.2779	$7.13^{+2.07}_{-1.66}$	$1.73^{+2.10}_{-1.03}$	$6.9^{+0.8}_{-0.5}$	6.50 ± 1.20	–
ABELL2645	0.2510	$4.16^{+1.15}_{-0.99}$	$3.58^{+2.30}_{-1.39}$	–	–	7.30 ± 1.53
ABELL2813	0.2924	$8.17^{+1.91}_{-1.61}$	$4.99^{+2.96}_{-1.83}$	–	5.48 ± 1.13	–
RXJ1504.1−0248	0.2153	$5.53^{+1.46}_{-1.25}$	$14.75^{+11.69}_{-5.44}$	$9.4^{+1.1}_{-1.0}$	–	15.31 ± 1.09
RXJ1720.1+2638	0.1640	$5.23^{+1.96}_{-1.45}$	$3.27^{+1.96}_{-1.31}$	$6.8^{+0.5}_{-0.3}$	7.46 ± 1.03	9.45 ± 0.48
RXJ2129.6+0005	0.2350	$4.69^{+1.63}_{-1.29}$	$1.44^{+1.51}_{-0.86}$	6.2 ± 0.6	7.62 ± 1.35	8.31 ± 0.44
ZwCl1021.0+0426	0.2906	$5.24^{+1.09}_{-0.96}$	$4.60^{+2.32}_{-1.52}$	–	10.48 ± 2.10	–
ZwCl1459.4+4240	0.2897	$8.54^{+1.22}_{-1.08}$	$3.91^{+0.92}_{-0.77}$	–	6.41 ± 2.76	–

are also implicit in the likelihood $\mathcal{L}_{\rm cluster}$ through the DfE term. $\mathcal{L}_{\rm clusters}$ is thus also multiplied by the product of the Gaussian likelihoods $\mathcal{L}_{H(z)} = \prod_i f_N(H(z_i)_{\rm predicted}; H(z_i), \sigma_{H(z_i)})$ of the $H(z)$ data and by the JLA likelihood $\mathcal{L}_{\rm JLA}$, based on estimates of binned distance modulus obtained from the JLA supernovae sample (from Betoule et al. 2014): $\mathcal{L}_{\rm total} = \mathcal{L}_{\rm clusters} \times \mathcal{L}_{H(z)} \times \mathcal{L}_{\rm JLA}$. An additional nuisance parameter ΔM is included to account for a possible shift in the absolute magnitudes of the supernovae.

We thus obtain the unnormalized posterior distribution probabilities $P(\theta|D)$, for our set of parameters $\theta = \{\xi, h, \Omega_{c0}h^2, \gamma, \Delta M\}$ given the data D by using Bayes' theorem

$$P(\theta \mid D) = \frac{\mathcal{L}_{\rm total}(D \mid \theta)\,\pi(\theta)}{P(D)}, \tag{26}$$

where $\pi(\theta)$ is the prior probability for the parameters, assumed flat and detailed in Section 4. The correct normalization of the posterior distribution is given by the marginal likelihood or evidence $P(D)$, which is not required for our parameter inference purposes.

4 THE MCMC ANALYSES

Using the EPIC code (Marcondes 2017), we run MCMC simulations for our interacting model with fixed $w_{\rm d} = -1$ using each of the four samples considered above and with $w_{\rm d}$ using the GOLD sample. The clusters data are combined with $H(z)$ and supernovae data in all cases. We set flat priors over the intervals $[-0.2, 0.2]$ for ξ, $[0.5, 0.9]$ for h, $[0.0, 0.3]$ for $\Omega_{c0}h^2$, $[0.00, 0.99]$ for γ, $[-1.0, 1.0]$ for ΔM and $[-2.0, -0.4]$ for $w_{\rm d}$ when it is

Table 2. Lognormal parameters (μ, σ) for measurements of masses (in units of $h^{-1}10^{14}M_\odot$), concentrations and temperatures (from Maughan et al. 2012, in keV) with asymmetrical uncertainties.

Cluster	M_{200}	c_{200}	k_BT_X
ABELL0068	(1.93, 0.19)	(1.67, 0.30)	(2.06, 0.13)
ABELL0115	(2.04, 0.31)	(0.68, 0.52)	(1.90, 0.04)
ABELL0209	(2.57, 0.16)	(1.34, 0.25)	(2.00, 0.07)
ABELL0267	(1.81, 0.19)	(1.22, 0.28)	(1.50, 0.10)
ABELL0383	(1.70, 0.22)	(1.56, 0.38)	(1.51, 0.07)
ABELL0521	(1.76, 0.20)	(1.37, 0.35)	(1.57, 0.04)
ABELL0586	(1.97, 0.27)	(2.26, 0.59)	(2.03, 0.11)
ABELL0697	(2.34, 0.25)	(0.72, 0.46)	(2.33, 0.07)
ABELL0750	(1.96, 0.32)	(1.56, 0.50)	–
ABELL0773	(2.27, 0.13)	(1.79, 0.24)	(2.00, 0.05)
ABELL0781	(1.94, 0.27)	(1.14, 0.62)	(1.73, 0.11)
ABELL0907	(2.74, 0.25)	(0.75, 0.41)	(1.69, 0.04)
ABELL0963	(1.99, 0.18)	(1.41, 0.30)	–
ABELL1423	(1.51, 0.24)	(1.89, 0.53)	–
ABELL1682	(2.18, 0.15)	(1.41, 0.23)	(1.85, 0.26)
ABELL1689	(2.42, 0.14)	(2.47, 0.31)	(2.14, 0.04)
ABELL1763	(2.86, 0.18)	(1.21, 0.30)	(2.09, 0.06)
ABELL1835	(2.34, 0.17)	(2.14, 0.41)	–
ABELL1914	(2.20, 0.20)	(1.06, 0.33)	(2.15, 0.06)
ABELL2009	(2.17, 0.31)	(0.94, 0.55)	–
ABELL2111	(1.77, 0.37)	(2.19, 0.91)	(1.87, 0.10)
ABELL2204	(2.30, 0.21)	(1.75, 0.32)	(2.14, 0.08)
ABELL2219	(2.38, 0.18)	(0.84, 0.40)	–
ABELL2261	(2.51, 0.16)	(1.07, 0.29)	(1.99, 0.05)
ABELL2390	(2.39, 0.17)	(1.46, 0.25)	–
ABELL2485	(1.78, 0.21)	(1.42, 0.44)	–
ABELL2537	(2.09, 0.26)	(2.60, 0.62)	–
ABELL2552	(2.12, 0.31)	(1.49, 0.62)	–
ABELL2631	(2.02, 0.25)	(0.96, 0.69)	(1.96, 0.09)
ABELL2645	(1.47, 0.25)	(1.48, 0.45)	–
ABELL2813	(2.14, 0.21)	(1.79, 0.42)	–
RXJ1504.1−0248	(1.76, 0.24)	(2.97, 0.47)	(2.25, 0.11)
RXJ1720.1+2638	(1.75, 0.31)	(1.36, 0.45)	(1.93, 0.06)
RXJ2129.6+0005	(1.62, 0.30)	(0.71, 0.67)	(1.83, 0.10)
ZwCl1021.0+0426	(1.69, 0.19)	(1.67, 0.38)	–
ZwCl1459.4+4240	(1.21, 0.29)	(2.81, 0.57)	–

free. The code evolved 12 independent Markov chains in each case, the convergence, according to the Gelman–Rubin criteria for multivariate distributions (Gelman & Rubin 1992; Brooks & Gelman 1998), being checked with the multivariate potential scale reduction factor $\hat{R}^p$ for p parameters within about 5×10^{-3} of 1.

The constraints on ξ and w_d are given in Table 3 at 1σ and 2σ confidence levels (CL); the other parameters are given in Table A1.

In Fig. 3, we plot the marginalized distributions of the parameters ξ, γ, and the joint-posterior distribution of ξ and w_d when this is also free, with the sample GOLD. We note that the analysis with w_d free has no effect on the marginalized distribution of the interaction constant (the corresponding violet and brown curves are almost indistinguishable), although it does affect the distribution of $\Omega_{c0}h^2$ (not plotted).

5 RESULTS

Constraints with sample M12+M16 are compatible with $\xi = 0$ within 1σ, while M12+M14, M14+M16, GOLD and GOLD with w_d free give 1.44σ, 2.30σ, 2.80σ, and 2.77σ detections, respectively. When we let the DE equation-of-state parameter vary,

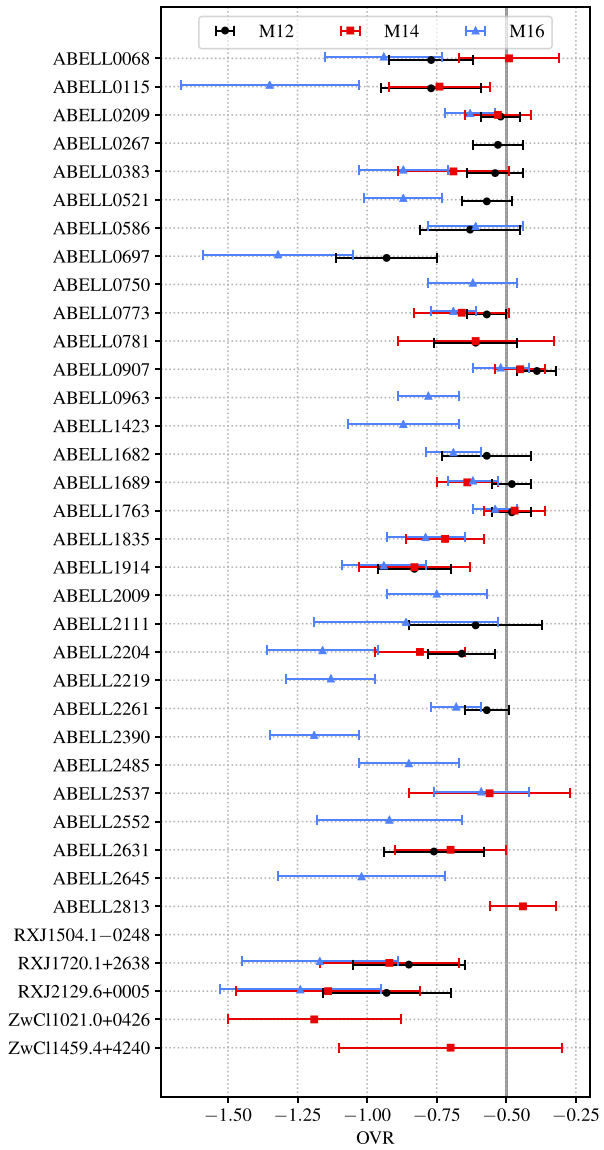

Figure 1. Processed OVRs from the NFW fit parameters data combined X-ray temperatures from different sources. The vertical grey line marks the classic value 0.5.

it can be noted from the joint-posterior distribution that w_d and ξ are not correlated; hence, the constraints on ξ (and also on all other parameters except $\Omega_{c0}h^2$) are practically unchanged. This can be seen in the lack of strong difference in Fig. 3 between the two GOLD distributions.

If we disregard the M12+M16 sample, as it only contains one cluster, it appears that we have 2σ to 3σ detection of the DE–DM interaction, a slight improvement on previous results of the virial detection idea (e.g. Bertolami et al. 2007). As discussed previously, the main problem appears from the inconsistent X-ray temperature detections, with no present guiding principle to favour one data set over another. We turned the difficulty by selecting in the three data sets available to us that contained consistent clusters and compiled them in a GOLD sample. The method clearly improves detection when stacking as many clusters as possible: the distribution of ξ on Fig. 3 is more peaked for larger samples.

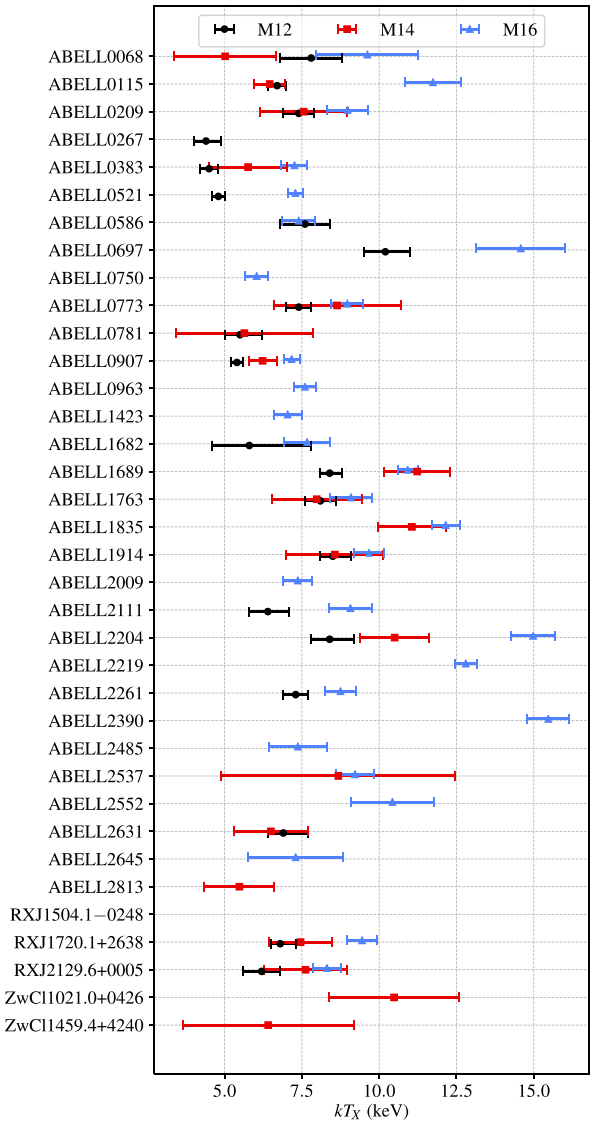

Figure 2. X-ray temperatures from different sources. Values are listed in Table 1.

Table 3. Constraints on the interaction strength parameter ξ and the derived parameter EVR(ξ) of the CDE model from $H(z)$ data, supernovae data and each of the clusters samples M12+M14, M12+M16, M14+M16 and GOLD.

Parameter	Sample	Best fitting	1σ CL	2σ CL
$100\,\xi$	M12+M14	-1.90	$-1.86^{+1.23}_{-1.28}$	$-1.86^{+2.62}_{-2.47}$
	M12+M16	-2.29	$-1.83^{+4.65}_{-4.43}$	$-1.83^{+10.42}_{-8.45}$
	M14+M16	-3.90	$-3.94^{+1.58}_{-1.44}$	$-3.94^{+3.38}_{-2.81}$
	GOLD	-2.85	$-2.70^{+0.90}_{-0.91}$	$-2.70^{+1.82}_{-1.81}$
	GOLD ($w_{\rm d}$ free)	-3.05	$-2.79^{+0.94}_{-0.93}$	$-2.79^{+1.97}_{-1.79}$
$w_{\rm d}$	GOLD ($w_{\rm d}$ free)	-0.98	$-0.99^{+0.16}_{-0.14}$	$-0.99^{+0.29}_{-0.32}$

6 DISCUSSION AND CONCLUSIONS

In this paper, we have continued the works of Bertolami et al. (2007), Le Delliou et al. (2007), Bertolami et al. (2008), Bertolami et al. (2009, 2012), Abdalla et al. (2009, 2010), He et al. (2010), Le Delliou et al. (2015) on virial detection of dark sector interaction. The approach of Le Delliou et al. (2015) for non-virialized clusters was improved to obtain consistent results. Based on evaluation of the dynamical out-of-equilibrium state independent of the details of each cluster's astrophysical history, the method relies on a set of simplifying reasonable assumptions. Although the convergence ansatz could be debatable, its general features prove to provide enough power to the method so as to be able to yield consistent results. From a sample of 50 clusters with full necessary data, consistency led us to trim down to a maximum of 11 clusters. The results range from no detection, but for a single cluster sample, to 3σ detection, with improvement when the samples are larger. This is a strong indication that the method is sound and likely to yield a clear answer to dark sector interaction question, given larger samples of clusters, with clear guidance on the X-ray temperature detection reliability and robust weak lensing determination.

This is why the detection of interaction in the dark sector (or its ruling out) will greatly benefit from future instruments and surveys. In particular, increasing the number of clusters with mass distribution measurements through lensing effects (which need deep imaging and large field of view) with the next generation of telescopes, such as the Thirty Meter Telescope (TMT; Skidmore & TMT International Science Development Teams & TMT Science

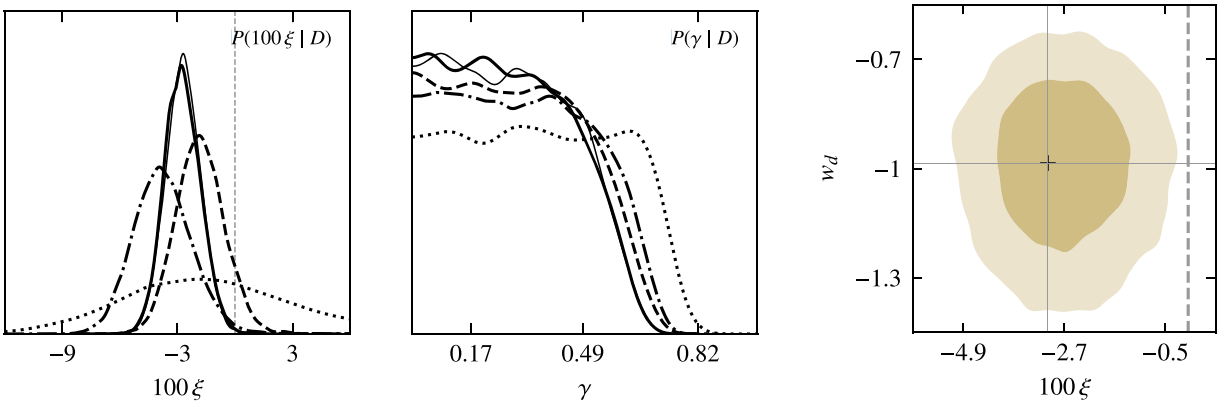

Figure 3. Marginalized distributions of ξ and γ for the samples M12+M14 (dashed), M12+M16 (dotted), M14+M16 (dash–dotted), GOLD with $w_{\rm d}$ fixed (solid, thin) and GOLD with $w_{\rm d}$ free (solid, thick). The dashed vertical line marks the no-interaction value $\xi = 0$. The last panel shows the two-dimensional joint-posterior distribution of the parameters ξ and $w_{\rm d}$ when this parameter is free, using the GOLD sample.

Advisory Committee 2015), the Giant Magellan Telescope (GMT; Johns et al. 2012) and the European Extremely Large Telescope (E-ELT; McPherson et al. 2012). Likewise, the X-ray detected clusters will increase in the next few years with the extended *ROentgen Survey with an Imaging Telescope Array* (*eROSITA*; Merloni et al. 2012). With these perspectives in observations and the method finalized here, we are confident that a reliable dark sector interaction detection is within reach.

ACKNOWLEDGEMENTS

We thank Dr. Nobushiro Okabe for generously sharing with us his NFW fits of the LoCuSS clusters. The work of MLeD. has been supported by Lanzhou University starting fund, the Fundamental Research Funds for the Central Universities (grant no. lzujbky-2019-25) and PNPD/CAPES20132029. MLeD also wishes to acknowledge DFMA/IF/USP and IFT/UNESP, where this work was initiated. GBLN thanks financial support from CNPq and FAPESP (2018/17543-0).

REFERENCES

Abdalla E., Abramo L. R., Sodré L., Wang B., 2009, Phys. Lett. B, 673, 107
Abdalla E., Abramo L. R., de Souza J. C. C., 2010, Phys. Rev. D, 82, 023508
Ade P. a. R. et al., 2014, A&A, 571, A16
Amendola L., 2000a, Phys. Rev. D, 62, 043511
Amendola L., 2000b, MNRAS, 312, 521
Amendola L. et al., 2013, Living Rev. Rel., 16,
Baldi M., 2012, MNRAS, 420, 430
Baldi M., Pettorino V., Robbers G., Springel V., 2010, MNRAS, 403, 1684
Bertolami O., Gil Pedro F., Le Delliou M., 2007, Phys. Lett. B, 654, 165
Bertolami O., Gil Pedro F., Le Delliou M., 2008, EAS Publ. Ser., 30, 161
Bertolami O., Gil Pedro F., Le Delliou M., 2009, Gen. Relativ. Gravit., 41, 2839
Bertolami O., Gil Pedro F., Le Delliou M., 2012, Gen. Relativ. Gravit., 44, 1073
Betoule M. et al., 2014, A&A, 568, A22
Böhmer C. G., Caldera-Cabral G., Lazkoz R., Maartens R., 2008, Phys. Rev. D, 78, 023505
Brooks S. P., Gelman A., 1998, J. Comput. Gr. Stat., 7, 434
Caldera-Cabral G., Maartens R., Schaefer B. M., 2009, J. Cosmol. Astropart. Phys., 0907, 027
Cao S., Liang N., 2013, Int. J. Mod. Phys. D, 22, 1350082
Clowe D., Bradač M., Gonzalez A. H., Markevitch M., Randall S. W., Jones C., Zaritsky D., 2006, ApJ, 648, L109
Costa A. A., Xu X.-D., Wang B., Abdalla E., 2017, J. Cosmol. Astropart. Phys., 1701, 028
Del Popolo A., 2009, ApJ, 698, 2093
Del Popolo A., Gambera M., Recami E., Spedicato E., 2000, A&A, 353, 427
Feng C., Wang B., Abdalla E., Su R., 2008, Phys. Lett. B, 665, 111
Gelman A., Rubin D. B., 1992, Stat. Sci., 7, 457
He J.-H., Wang B., Abdalla E., Pavon D., 2010, J. Cosmol. Astropart. Phys., 1012, 022
He J.-H., Wang B., Abdalla E., 2011, Phys. Rev. D, 83, 063515
Henriksen R. N., Widrow L. M., 1995, MNRAS, 276, 679
Henriksen R. N., Widrow L. M., 1997, Phys. Rev. Lett., 78, 3426
Henriksen R. N., Widrow L. M., 1999, MNRAS, 302, 321
Jee M. J., Hughes J. P., Menanteau F., Sifón C., Mandelbaum R., Barrientos L. F., Infante L., Ng K. Y., 2014, ApJ, 785, 20
Johns M. et al., 2012, Proc. SPIE, 8444, 84441H
Le Delliou M., 2008, A&A, 490, L43
Le Delliou M., Barreiro T., 2013, J. Cosmol. Astropart. Phys., 1302, 037
Le Delliou M., Henriksen R. N., 2003, A&A, 408, 27
Le Delliou M., Bertolami O., Gil Pedro F., 2007, AIP Conf. Proc., 957, 421
Le Delliou M., Marcondes R. J. F., Lima Neto G. B., Abdalla E., 2015, MNRAS, 453, 2(LeD15)
Li B., Barrow J. D., 2011a, Phys. Rev. D, 83, 024007
Li B., Barrow J. D., 2011b, MNRAS, 413, 262
Liao S., Gao L., Frenk C. S., Guo Q., Wang J., 2017, MNRAS, 470, 2262
Li Y.-H., Zhang X., 2011, Eur. Phys. J. C, 71, 1700
Macciò A., Quercellini C., Mainini R., Amendola L., Bonometto S., 2004, Phys. Rev. D, 69, 123516
MacMillan J. D., Widrow L. M., Henriksen R. N., 2006, ApJ, 653, 43
Mainini R., 2005, Phys. Rev. D, 72, 083514
Mainini R., Bonometto S., 2006, Phys. Rev. D, 74, 043504
Majerotto E., Väliviita J., Maartens R., 2010, MNRAS, 402, 2344
Mantz A. B. et al., 2016, MNRAS, 463, 3582(M16)
Mantz A. B. et al., 2017, MNRAS, 467, 3443
Marcondes R. J. F., 2017, preprint (astro-ph.IM/1712.00263)
Martino R., Mazzotta P., Bourdin H., Smith G. P., Bartalucci I., Marrone D. P., Finoguenov A., Okabe N., 2014, MNRAS, 443, 2342(M14)
Maughan B. J., Giles P. A., Randall S. W., Jones C., Forman W. R., 2012, MNRAS, 421, 1583(M12)
McPherson A., Spyromilio J., Kissler-Patig M., Ramsay S., Brunetto E., Dierickx P., Cassali M., 2012, in Proc. SPIE, 8444, 84441F
Merloni A. et al., 2012, preprint (astro-ph.HE/1209.3114)
Monteiro-Oliveira R., Cypriano E. S., Machado R. E. G., Lima Neto G. B., Ribeiro A. L. B., Sodré L., Dupke R., 2017, MNRAS, 466, 2614
Moresco M. et al., 2016, J. Cosmol. Astropart. Phys., 1605, 014
Navarro J. F., Frenk C. S., White S. D. M., 1996, ApJ, 462, 563
Okabe N., Smith G. P., 2016, MNRAS, 461, 3794
Perlmutter S. et al., 1999, ApJ, 517, 565
Rasia E., Tormen G., Moscardini L., 2004, MNRAS, 351, 237
Riess A. G. et al., 1998, AJ, 116, 1009
Riess A. G. et al., 2016, ApJ, 826, 56
Salvatelli V., Marchini A., Lopez-Honorez L., Mena O., 2013, Phys. Rev. D, 88, 023531
Skidmore W., TMT International Science Development Teams, TMT Science Advisory Committee, 2015, Res. Astron. Astrophys., 15, 1945
Wang B., Abdalla E., Atrio-Barandela F., Pavón D., 2016, Rep. Prog. Phys., 79, 096901
Zwicky F., 1933, Helv. Phys. Acta, 6, 110
Zwicky F., 1937, ApJ, 86, 217

APPENDIX: CONSTRAINTS ON THE OTHER PARAMETERS

Completing Table 3, we present here in Table A1 the remaining constraints on the other parameters of our analyses. The confidence intervals reported for γ without central values reflect the fact that its distributions are poorly constrained, only suppressed by the singularity as γ approaches 1 but otherwise flat. The exact values at which the distributions become suppressed are sensitive to our arbitrary choice of $t_0 = 1\,\mathrm{km}^{-1}\,\mathrm{s\,Mpc}$ (see Section 2.2.2). However, this does not affect our results, which are based on marginalizing this parameter over all values allowed by our priors. Constraints on the parameters Ω_{c0} and Ω_{d0} derived from $\Omega_{c0}h^2$ and h are also listed.

Table A1. Constraints on parameters of CDE model from $H(z)$ data, supernovae data and each of the clusters samples M12+M14, M12+M16, M14+M16, and GOLD.

Parameter	Group	Best fitting	1σ CL	2σ CL
h	M12+M14	0.72	$0.72^{+0.01}_{-0.02}$	$0.72^{+0.02}_{-0.03}$
	M12+M16	0.72	$0.71^{+0.02}_{-0.01}$	$0.71^{+0.03}_{-0.02}$
	M14+M16	0.71	$0.72^{+0.01}_{-0.02}$	$0.72^{+0.02}_{-0.03}$
	GOLD	0.71	$0.71^{+0.02}_{-0.01}$	$0.71^{+0.03}_{-0.02}$
	GOLD ($w_{\rm d}$ free)	0.71	$0.71^{+0.02}_{-0.01}$	$0.71^{+0.03}_{-0.02}$
$\Omega_{c0}h^2$	M12+M14	0.13	$0.13^{+0.02}_{-0.01}$	$0.13^{+0.03}_{-0.02}$
	M12+M16	0.13	$0.13^{+0.03}_{-0.02}$	$0.13^{+0.06}_{-0.03}$
	M14+M16	0.13	0.13 ± 0.01	0.13 ± 0.02
	GOLD	0.13	0.13 ± 0.01	0.13 ± 0.02
	GOLD ($w_{\rm d}$ free)	0.14	$0.15^{+0.02}_{-0.03}$	$0.15^{+0.04}_{-0.07}$
γ	M12+M14	0.03	$0 < \gamma \leq 0.41$	$0 < \gamma \leq 0.61$
	M12+M16	0.20	$0 < \gamma \leq 0.64$	$0 < \gamma \leq 0.71$
	M14+M16	0.10	$0 < \gamma \leq 0.43$	$0 < \gamma \leq 0.63$
	GOLD	0.01	$0 < \gamma \leq 0.39$	$0 < \gamma \leq 0.57$
	GOLD ($w_{\rm d}$ free)	0.11	$0 < \gamma \leq 0.38$	$0 < \gamma \leq 0.57$
ΔM	M12+M14	0.04	0.04 ± 0.04	$0.04^{+0.08}_{-0.09}$
	M12+M16	0.04	0.04 ± 0.04	$0.04^{+0.08}_{-0.09}$
	M14+M16	0.03	$0.03^{+0.05}_{-0.04}$	$0.03^{+0.09}_{-0.08}$
	GOLD	0.03	0.04 ± 0.04	$0.04^{+0.08}_{-0.09}$
	GOLD ($w_{\rm d}$ free)	0.04	0.04 ± 0.04	0.04 ± 0.09
Ω_{c0}	M12+M14	0.26	$0.26^{+0.03}_{-0.02}$	$0.26^{+0.06}_{-0.05}$
	M12+M16	0.26	$0.26^{+0.05}_{-0.04}$	$0.26^{+0.12}_{-0.07}$
	M14+M16	0.25	$0.25^{+0.02}_{-0.03}$	0.25 ± 0.05
	GOLD	0.25	$0.26^{+0.02}_{-0.03}$	$0.26^{+0.04}_{-0.05}$
	GOLD ($w_{\rm d}$ free)	0.28	$0.29^{+0.04}_{-0.06}$	$0.29^{+0.09}_{-0.13}$
Ω_{d0}	M12+M14	0.74	$0.74^{+0.02}_{-0.03}$	$0.74^{+0.05}_{-0.06}$
	M12+M16	0.74	$0.74^{+0.04}_{-0.05}$	$0.74^{+0.07}_{-0.12}$
	M14+M16	0.75	$0.75^{+0.03}_{-0.02}$	0.75 ± 0.05
	GOLD	0.75	$0.74^{+0.03}_{-0.02}$	$0.74^{+0.05}_{-0.04}$
	GOLD ($w_{\rm d}$ free)	0.72	$0.71^{+0.06}_{-0.04}$	$0.71^{+0.13}_{-0.09}$

This paper has been typeset from a TEX/LATEX file prepared by the author.